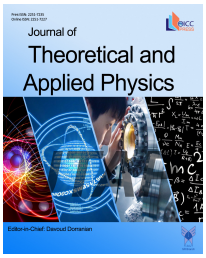

Volume 18, Issue 4, 182448 (1-12)

Journal of Theoretical and Applied Physics (JTAP)

https://dx.doi.org/10.57647/j.jtap.2024.1804.48

A comparative study on predicting the characteristics of plasma activated water: artificial neural network (ANN) & support vector regression (SVR)

Saeed Karimian[1], Shahrzad Falahat[2], Zahra Emam Bakhsh[1], Mohammad Javad Ghavami Rad[3], Ali Barkhordari[2,*]

[1]*Department of Physics, Vali-e-Asr University of Rafsanjan, Rafsanjan, Iran.*
[2]*Faculty of Physics, Shahid Bahonar University of Kerman, Kerman, Iran.*
[3]*Faculty of Sciences, Center Branch of Tehran, Islamic Azad University, Tehran, Iran.*

[*]**Corresponding author:** alibarkhordari20@yahoo.com

Original Research

Received:
21 February 2024
Revised:
8 May 2024
Accepted:
16 May 2024
Published online:
30 August 2024

Abstract:

In this paper, the applicability of the Machine Learning (ML) technique in predicting the structural characteristics of water exposed by the plasma discharge is studied. For this purpose, the structural characteristics of water including pH, Electrical Conductivity (EC), Oxidation Reduction Potential (ORP), Total Dissolved Solution (TDS), and salt is experimentally measured before and after exposing the plasma. The plasma discharge medium consists of air and water. The applied voltage and the time duration of plasma application are considered as operational variables. Also, Support Vector Regression (SVR), as a strong algorithm of Machine Learning (ML), is applied on the data to train a model for accurately predicting the water characteristics as the new data. It is shown that pH value is reduced at higher applied voltages and time of plasma treatment while EC, ORP, TDS, and salt are increased. It was also found that the SVR model can predict the main characteristics of water with a high $R2$ score of 0.998. The results obtained by SVR in the prediction of water characteristics are compared with the performance of Artificial Neural Network (ANN) as another interesting ML algorithm, showing the better performance of the SVR algorithm than ANN one.

Keywords: Plasma discharge; Water characteristics; Machine Learning (ML); Support Vector Regression (SVR); Artificial Neural Network (ANN)

1. Introduction

Recently, one of the attractive points in the field of plasma science and technology is plasma-liquid interactions [1–3]. The application areas of the interactions of non-equilibrium plasmas with liquids are extended from environmental remediation and material science to sterilization and medicine [4–7].

Generally, when a non-equilibrium plasma interacts with a liquid, the changes in the creation of reactive oxygen and nitrogen species (RONS) and hence in the electrical conductivity and redox potential are occurred because of the acidification of the environment. So, this plasma activated water (PAW) contains various chemical compositions than the pure water and is able to use as an alternative technique for microbial decontamination [7–14].

Not only does PAW seem to have a synergetic impact on decontamination, but it could also improve the growth of seeds. The improvement of plant growth is because of increasing the nitrite and nitrate ions in PAW. So, soaking seeds in PAW elevates seed germination and plant growth while being anti-bacterial. Moreover, it is able to be applied for enhancing product efficiency and for fighting against dryness-stress in the environment [8].

Bruggeman et al. presented the electrical and optical features of a plasma made between a liquid cathode and a metal anode. They found that the plasma has gathered contiguity points at the liquid cathode and obviously filamentary close to the water surface. On the other hand, the voltage

decline of cathode relates to the electrical conductivity than pH value and was remarkably various for distilled water and electrolyte solutions [13]. ML, as a subset of artificial intelligence, is a powerful tool to analyze data samples and build some patterns and rules to evolve a simulation scheme, resulting in predicting future data. ML does not need human interventions while accomplishing predictive processes with high accuracy [15]. There is a wide variety of algorithms contributed to ML modeling to train the rules and then predict the new data. Two of the advanced algorithms of ML are the SVR and ANN because it has a strong training structure and accurate prediction abilities [16].

In this paper, the characteristics of water are investigated when it is a part of plasma discharge medium at atmospheric pressure. The plasma discharge is included the air and water, between a pin placed on above the water surface and a ring put on the bottom of water. First, the main characteristics of water including pH, EC, ORP, TDS, and salt are measured by applying the voltage and during the treatment time. Next, the physical reasons behind the variations of these factors are discussed in detail. Then, the SVR and ANN algorithms are used to analyze the data and implement a structure for predicting the new data. Finally, the performance of the SVR algorithm is compared to ANN model.

2. Experimental details

2.1 Experimental setup

To provide the power needed for triggering an electric discharge plasma, a Tesla coil system with a voltage from 30 to 40 kV at 60 kHz fixed frequency was designed and manufactured. A schematic diagram of the experimental setup has been shown in Figure 1. An aluminum needle (powered) electrode with 2 mm diameter was placed at the distance of 1 cm above a water surface the other aluminum ring electrode (grounded) in water, respectively. The spatial distance between two electrodes was constant. In fact, the changeability of the applied voltages and time allows us to study the changes in the structural parameters of water.

It must be noted that, first the structural characteristics of water including pH, ORP, EC, TDS, and salt of water are measured using a pH spear, ORP tester HI98201, EC meter model 8200, respectively. The measured pH values before the effect of plasma at 25 C are equal to 7.

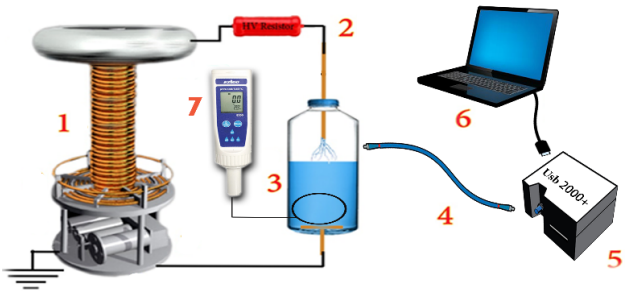

Figure 1. Schematic of the experimental setup; 1) High voltage source (Tesla coil device), 2) High voltage resistance, 3) Water chamber, 4) Optical fiber, 5) Spectrometer, 6) Computer, 7) EC meter device.

In this work, the operational conditions such as the applied voltage and the time duration of plasma application are varied and their effects on the structural characteristics of water are examined. In order to analyze the data and to predict the new data, SVR is used as an accurate and strong algorithm of ML and the obtained results are compared to ANN.

2.2 Support vector regression (SVR) algorithm

Given a training dataset $T = \{(x_1, y_1),\ldots,(x_N, y_N)\}$, which consists of N ordered pairs of (x_i, y_i) for $i = 1, 2, ..., N$, where x_i and y_i represent the features and their corresponding target values, respectively, the main purpose of implementing SVR is to find a smooth regression profile $f(x)$ with the minimum deviation ε value between the predicted and target values for all the data in the training set. The estimation function of the SVR algorithm, $f(x)$, can be expressed as follows [15]:

$$f(x) = w^T \varphi(x) + b \tag{1}$$

where w refers to the weight vector, $\varphi(x)$ denotes the feature function of input x, and b being a constant. To find optimal regression function, we must solve the convex optimization problem given by [15]:

$$\min \ \frac{1}{2}\|w\|^2 \qquad s,t, \begin{cases} y_i - w^T \varphi(x_i) - b \le \varepsilon \\ w^T \varphi(x_i) + b - y_i \le \varepsilon \end{cases} \tag{2}$$

Maybe, the function, $f(x)$, that satisfies these constraints at all points could not be acquired. We can present ξ_i and ξ_i^*, positive and negative slack parameters at each point, to address infeasible constraints while still meeting the necessary requirements [16]:

$$\min \ \frac{1}{2}\|w\|^2 + C\,\Sigma_{i=1}^{N}(\xi_i + \xi_i^*) \qquad s,t, \begin{cases} y_i - w^T \varphi(x_i) - b \le \varepsilon + \xi_i \\ w^T \varphi(x_i) + b - y_i \le \varepsilon + \xi_i^* \end{cases} \tag{3}$$

With C being a penalty factor that is carefully chosen to balance the complexity of the model and the error of the training set, thus avoiding overfitting. Additionally, ξ_i and ξ_i^* must be greater than or equal to 0 for all i. In order to solve this optimization problem, it can be transformed into dual problem after applying the Karush-Kuhn-Tucker (KKT) condition as [17]:

$$\begin{aligned} \max \ -\frac{1}{2}\Sigma_{i,j=1}^{N}(\beta_i - \beta_i^*)(\beta_j - \beta_j^*)\varphi(x_i)^T\varphi(x_j) - \\ \varepsilon\Sigma_{i=1}^{N}(\beta_i + \beta_i^*) + \Sigma_{i=1}^{N} y_i(\beta_i - \beta_i^*) \\ s,t, \{\Sigma_{i=1}^{N}(\beta_i - \beta_i^*) = 0 \end{aligned} \tag{4}$$

With β_i and $\beta_i^* \in [0, C]$ being the Lagrange multipliers. So, the SVR function is given by [16]:

$$f(x) = \Sigma_{i=1}^{N}(\beta_i - \beta_i^*)k(x_i, x_j) + b \tag{5}$$

with $k(x_i, x_j) = \varphi(x_i)^T\varphi(x_j)$ being the kernel function allowing us to linearly solve the non-linear problems [17].

Different kernel functions are available to use such as linear, polynomial, sigmoid, and Radial Basis Function (RBF) [15–17]. This work has chosen Radial Basis Function (RBF) as its kernel function due to its fewer factors and numerical simplicity. Therefore, it is defined as [16, 17]:

$$k(x_i, x_j) = \exp(-\gamma \|x_i - x_j\|^2) \quad (6)$$

with γ being the kernel width. The SVR model is designed in three steps. The first step in designing an SVR model is determining the hyperparameters that form the model (see Table 1). The next step in designing an SVR model is to analyze and evaluate its training and prediction performance. Finally, the validated model has yielded the anticipated prediction data.

2.3 Artificial neural network (ANN) model

Artificial Neural Networks (ANNs) inspired from the human's brain. They use different mathematical layers to process the information it's fed. ANNs typically have a large number of artificial neurons, called units, arranged in a series of layers [18]. The input layer receives data that the network learns. From the input layer, data comes from one or more hidden layers. A hidden layer transforms the input into something that the output layer can use by utilizing different mathematical processes [18]. Most neural networks are fully connected from one layer to another. Data can learn more as it passes through each network layer. At the output layer, the network responds with the data it receives. The ANN training process consists of two parts. First, in the feed-forward stage, data moves from the input layer to the output layer through all hidden layers. In this stage, the neurons process the input and return the output using an activation function. The activation function helps the network to learn the complex patterns of the data by changing the output to a nonlinear form [19]. After that, the reverse process is performed. This stage which is called back-propagation adjusts the weights and biases of all nodes by minimizing the loss between the actual and predicted values by the network.

The forward and backward processes are repeated until the network trains completely and the optimized values of parameters obtains. The trained network can predict the output accurately. For each node per layer, the output function can be expressed as described by [18, 19];

$$y_i = \Sigma_{i=1}^{n} f(w_i * x_i + b) \quad (7)$$

where x_i is the node's input vector, b is the bias value, w_i represents the weight vector of the node, and f is the activation function. Rectified Linear Unit (ReLU), Leaky ReLU, tanh, softmax, and sigmoid are the most important activation functions that can be used [18, 19].

2.4 Error and accuracy functions

It is essential to conduct a thorough analysis of the predictive capabilities of the SVR model once the design is complete. By calculating performance factors and then analyzing them, we can gain insight into the accuracy of our predictions. The accuracy of the SVR model employed in this work is evaluated using two metrics: mean absolute error (MAE) and determination coefficient (R). These parameters are defined as follows [20, 21]:

$$\text{MAE} = \frac{1}{N} |X_{\text{exp}(i)} - X_{\text{pred}(i)}| \quad (8)$$

$$R2 \text{ Score} = 1 - \frac{\Sigma_{i=1}^{N} (X_{\text{pred}(i)} - X_{\text{exp}(i)})^2}{\Sigma_{i=1}^{N} (\bar{X}_{\text{exp}(i)} - X_{\text{exp}(i)})^2} \quad (9)$$

where X_{pred} is the prediction value by the model, X_{exp} is the experimental value (actual value), and $\bar{X}_{\text{exp}}$ is the average value of the experimental data. The obtained values of MAE and $R2$ score as a result of predicting each parameter of water in terms of applied voltages and treatment time of plasma by the SVR algorithm is presented in Table 1. Both MAE and $R2$ functions for the water parameters have good values implying that the SVR model is an accurate and reliable algorithm for predicting the water parameters. The smallest and largest values of the voltage-dependent MAE function are 0.06 for pH and 6.72 for ORP, respectively. These values correspond to 0.07 for pH and 3.54 for conductivity when the MAE function depends on the treatment time of the plasma. Moreover, the error and accuracy functions of ANN algorithm in the prediction of the water parameters in terms of applied voltages and treatment time of plasma are introduced in Table 2. Similar to the previous case, the MAE and $R2$ functions in the ANN-based predictions of water parameters show that the ANN algorithm only

Table 1. Error and accuracy functions in SVR-based predictions.

Variables (Parameters)	Voltage		Time	
	MAE	$R2$	MAE	$R2$
EC	3.77	0.94	3.54	0.99
ORP	6.72	0.93	3.50	0.96
pH	0.06	0.79	0.07	0.97
Salt	1.37	0.97	1.36	0.99
TDS	1.60	0.96	1.98	0.99

Table 2. Error and accuracy functions in ANN-based predictions.

Variables (Parameters)	Voltage		Time	
	MAE	$R2$	MAE	$R2$
EC	3.06	0.99	4.58	0.99
ORP	6.72	0.93	5.13	0.91
pH	0.04	0.93	0.04	0.91
Salt	3.66	0.81	3.33	0.99
TDS	2.43	0.96	2.12	0.99

predicts the voltage-dependent conductivity better than the SVR model, and it shows the higher values of MAE functions in the prediction of other water parameters compared to the SVR algorithm.

2.5 Hyperparameters setting

Hyperparameter setting of SVR and ANN methods for voltage and time variables are respectively represented in Tables 3 and 4.

C, gamma, and kernel are essential hyperparameters in SVR. The *C* parameter controls the trade-off between fitting the training data closely and preventing overfitting. A smaller *C* value encourages simpler models with more regularization, while a larger *C* value reduces regularization, leading to a closer fit to the training data. The gamma parameter determines the influence of individual training samples on the decision boundary.

A smaller gamma value results in a wider decision boundary with a more generalized model, while a larger gamma value creates a narrower decision boundary that focuses on nearby data points. The kernel parameter defines the type of kernel function used, enabling the model to capture complex relationships in the data.

In this table, the hidden layer sizes parameter determines the architecture of the model, specifying the number of neurons in each hidden layer. By adjusting the size and number of hidden layers, the complexity and capacity of the model can be controlled. The activation function applied to the hidden layers, enabling the model to capture nonlinear relationships within the data. Additionally, the solver parameter determines the optimization algorithm used during training, impacting convergence speed and performance. Also, the learning rate determines the step size used to update the model's weights during the optimization process.

Figure 2 illustrates the variations of *R*2 score function as a function of the hyperparameters used in the SVR ML algorithm, i.e., *C* and γ, when the water parameters are voltage-dependent. As seen, the *R*2 score function for the prediction of all the water parameters is maximized by increasing the γ value when the value of *C* is from 10^{-1} to

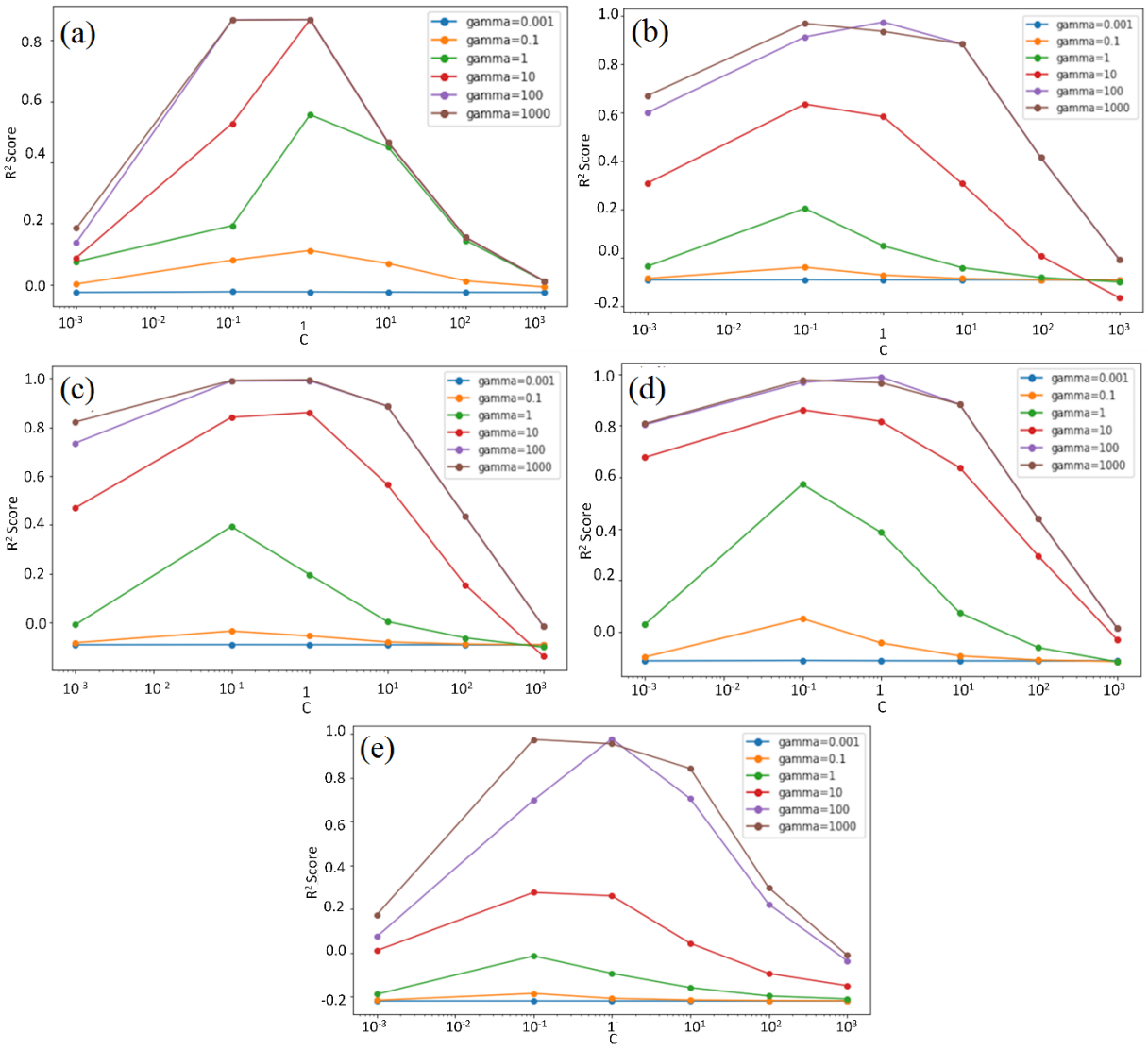

Figure 2. Changes of the *R*2 score versus the hyperparameters (C & γ) in the SVR model for the voltage-dependent (a) pH, (b) EC, (c) TDS, (d) salt, and (e) ORP.

10. The changes of $R2$ score function depending on the hyperparameters applied for implementing the SVR ML model are represented in Figure 3. The water parameters are in terms of treatment time of plasma in this figure. It is obvious that the value of $R2$ score is reduced by growing both C and γ up in the prediction of all the water parameters.

Table 3. Hyperparameter setting of SVR algorithm.

Variables	Kernel	C	Gamma
Voltage	Gaussian	1	10 e2
Time	Gaussian	10 e-1	10 e-2

3. Results and discussion

If a high voltage is applied on the electrodes, time is one of the most important factors changing the water characteristics, i.e., pH, EC, TDS, salt, and ORP. In order to carry out the experiment, the water volume of 250 cc, the 6 cm distance between electrodes, and 12 kV applied voltage have been considered. It should be mentioned that the distance of the pin from the surface of water was equal to 2 cm. Additionally, the variations of water properties were measured at an interval of [0-27] minutes by the 5-second step. It must be noted that the initial values of pH, EC, TDS, salt, and ORP were 7, 35 μs, 19 ppm, 11 ppm, and 21 mV, respectively. After applying the voltage on the electrodes, the plasma discharge is triggered in the air gap and into the water that causes the interactions between the gas phase and

Table 4. Hyperparameter setting of ANN model.

Variables	Hidden layer sizes	Activation function	Solver Solver	Learning rate
Voltage	100	tanh	lbfgs	1 e-3
Time	100	tanh	lbfgs	1 e-3

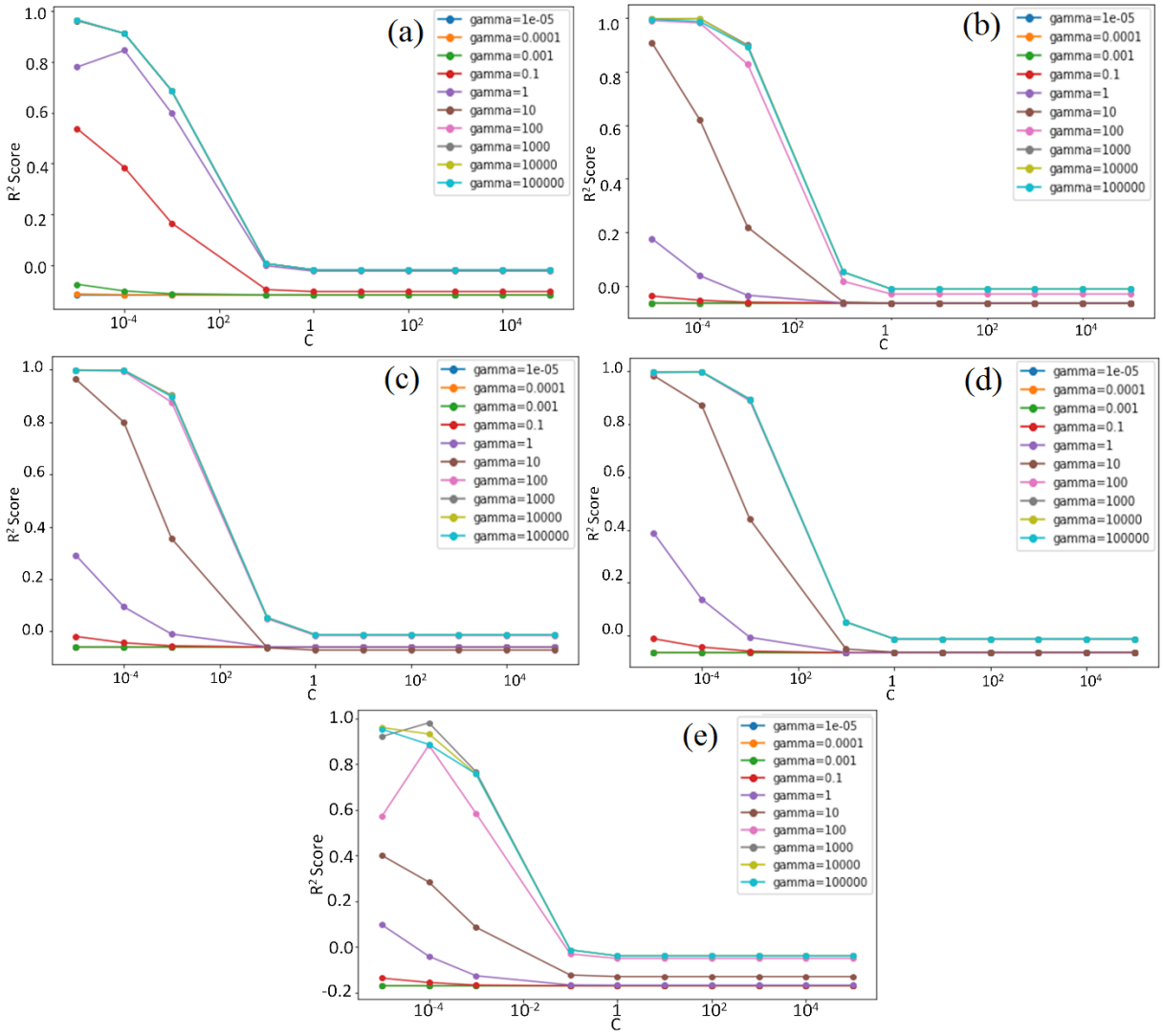

Figure 3. Variations of the $R2$ score as a function of the hyperparameters (C & γ) in the SVR algorithm for the time-dependent (a) pH, (b) EC, (c) TDS, (d) salt, and (e) ORP.

liquid phase (water) with a volume of 250 cc. The RONS are created in the plasma region and therefore, these charged particles cause to increase the EC and ORP of the water from 35 μs and 21 mV to 446 μs and 262 mV, respectively (see Figure 4 (b) and 4 (e)). On the other hand, some of the RONS such as H_3O^+, NO_2^-, and NO_3^- molecular species produced in the plasma region give rise to acidification of water, resulting in decreasing the pH value of water [22, 23]. As can be seen in Figure 4 (a), the pH value was equal to 3.46 after 27 min. Moreover, the TDS and salt are also increased by growing the interactions up in the plasma region during the treatment time whose value is equal to 291 ppm and 220 ppm after 27 min, respectively (see Figure 4 (c) and 4 (d)).

As known, the electric field is becoming stronger in the plasma medium by increasing the voltage applied on the electrodes. The charged particles get more accelerated in this stronger field, and as a result, the ionizing collisions in-

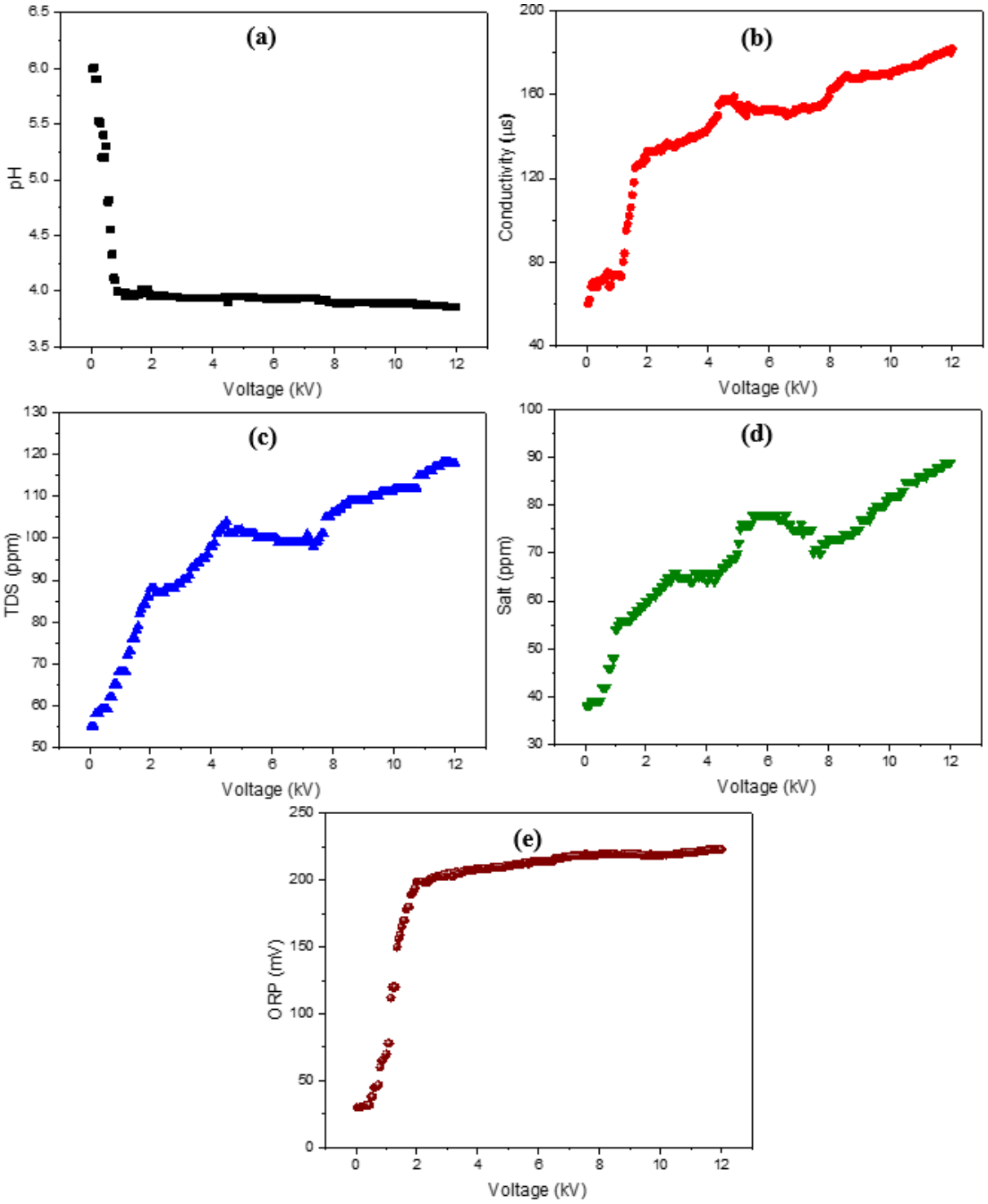

Figure 4. Variations of (a) pH, (b) EC, (c) TDS, (d) salt, and (e) ORP as a function of time in the water volume of 250 cc at the applied voltage of 12 kV.

crease between charged and neutral particles [24, 25]. The RONS in the plasma medium are becoming more and more by growing applied voltage up. So, the interactions between the RONS and water molecules are raised and the water characteristics change. The experiments were repeated by changing the voltage applied on the electrodes from 50 V to 12 kV at the electrode distance at 6 cm with the volume of water 250 cc and the water characteristics have been measured after 27 min. It is observable that the pH value is decreased by raising the applied voltage while other factors, i.e., ORP, EC, TDS, salt, grown up as shown in Figure 5. It is clear that the pH value is approximately constant after the applied voltage of 1 kV and the time of 13 minute. In many cases, rate coefficients are frequently reported for buffered solutions, maintaining a constant pH level, such as in nitric acid buffered solutions where there is an assumption of an

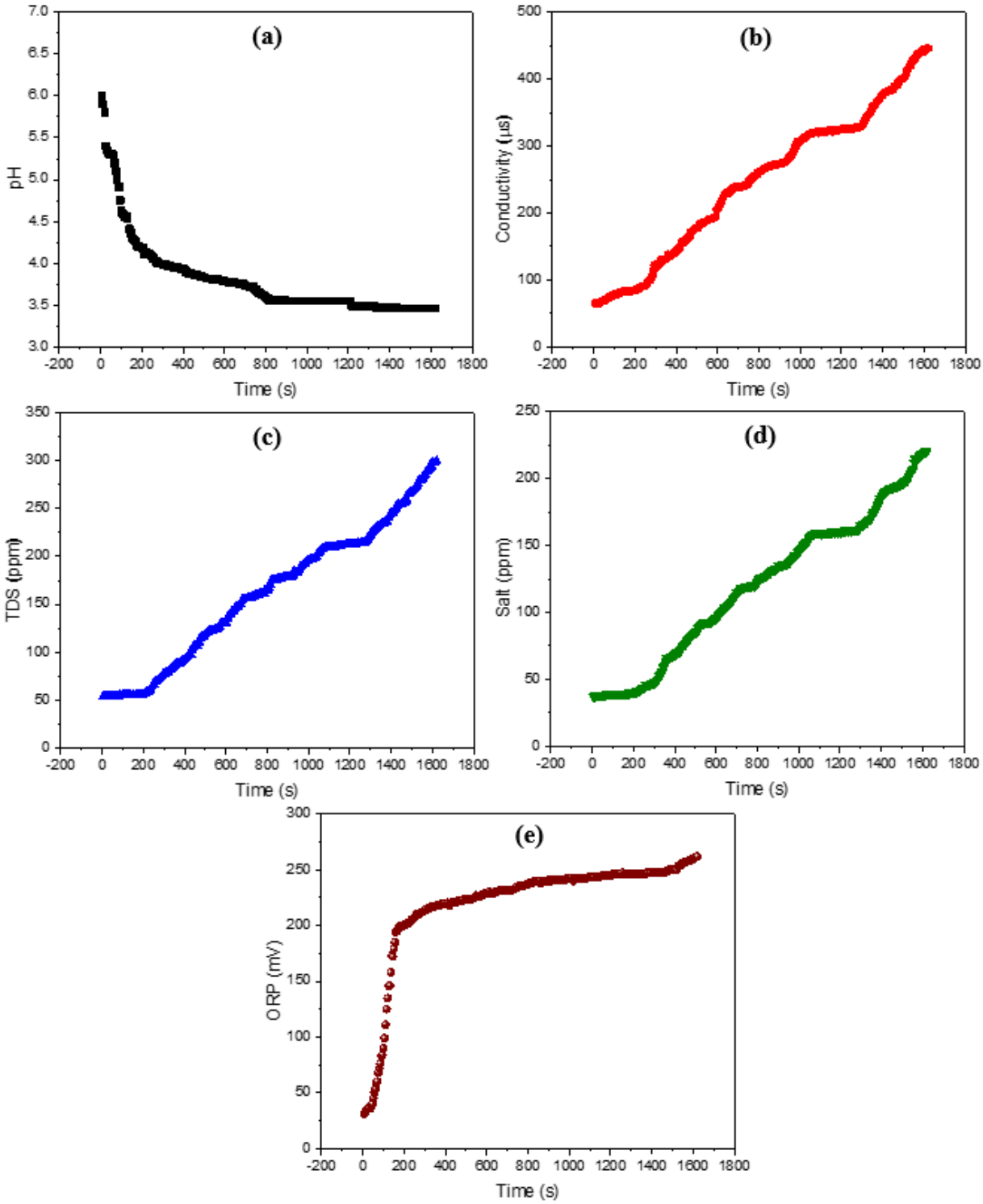

Figure 5. Variations of (a) pH, (b) EC, (c) TDS, (d) salt, and (e) ORP versus of applied voltage in the water volume of 250 cc after 27 min.

abundant reservoir of H_3O^+ and NO_3^-. It is worth noting that, in the context of electrochemistry literature, H_3O^+ is commonly denoted as H^+ with the understanding that it is hydrated (though the notation H_3O^+ is employed in this paper). The pH of a solution is commonly expressed as $pH = \log_{10}[H_3O^+]$, with $[H_3O^+]$ indicating the molar concentration (mol/L). Hence, a pH-sensitive rate coefficient represents a multi-body rate coefficient where the consistently present H_3O^+ density is not explicitly mentioned. Considering that plasma treatment of liquids can alter the pH by generating H_3O^+, reaction rate coefficients affected by pH should be articulated as a function of hydronium $[H_3O^+]$, thereby linking these coefficients implicitly to the prevailing conditions. Numerous reaction rates are exclusively given for particular pH values. On the other hand, the increase of the charged particles, i.e., electrons, positive and negative ions, in the water results in raising the electrical conductivity and oxidation-reduction potential. Moreover, the reactions in the water lead to decomposing chemical species, increasing the reactive species. So, the total dissolved solution and salt will be raised in the water. Similar results have been reported in the literature [26–35].

On the other hand, the actual values of pH, EC, TDS, salt, and ORP are compared by their corresponding predicted values with the SVR and ANN algorithms in Figures 6 and 7. The *x*- and *y*-axis correspond to the experimental and predicted data. For a better understanding of the prediction accuracy, it needs to be estimated the locations of data points, and to this purpose, the zero-error line has been drawn in Figures 6 and 7. The comparison of the data points of the SVR and ANN models to the zero-error line reveals that the SVR model is more accurate in predicting the water characteristics in terms of the applied voltage (see Figure 6) and time (see Figure 7) than the ANN model.

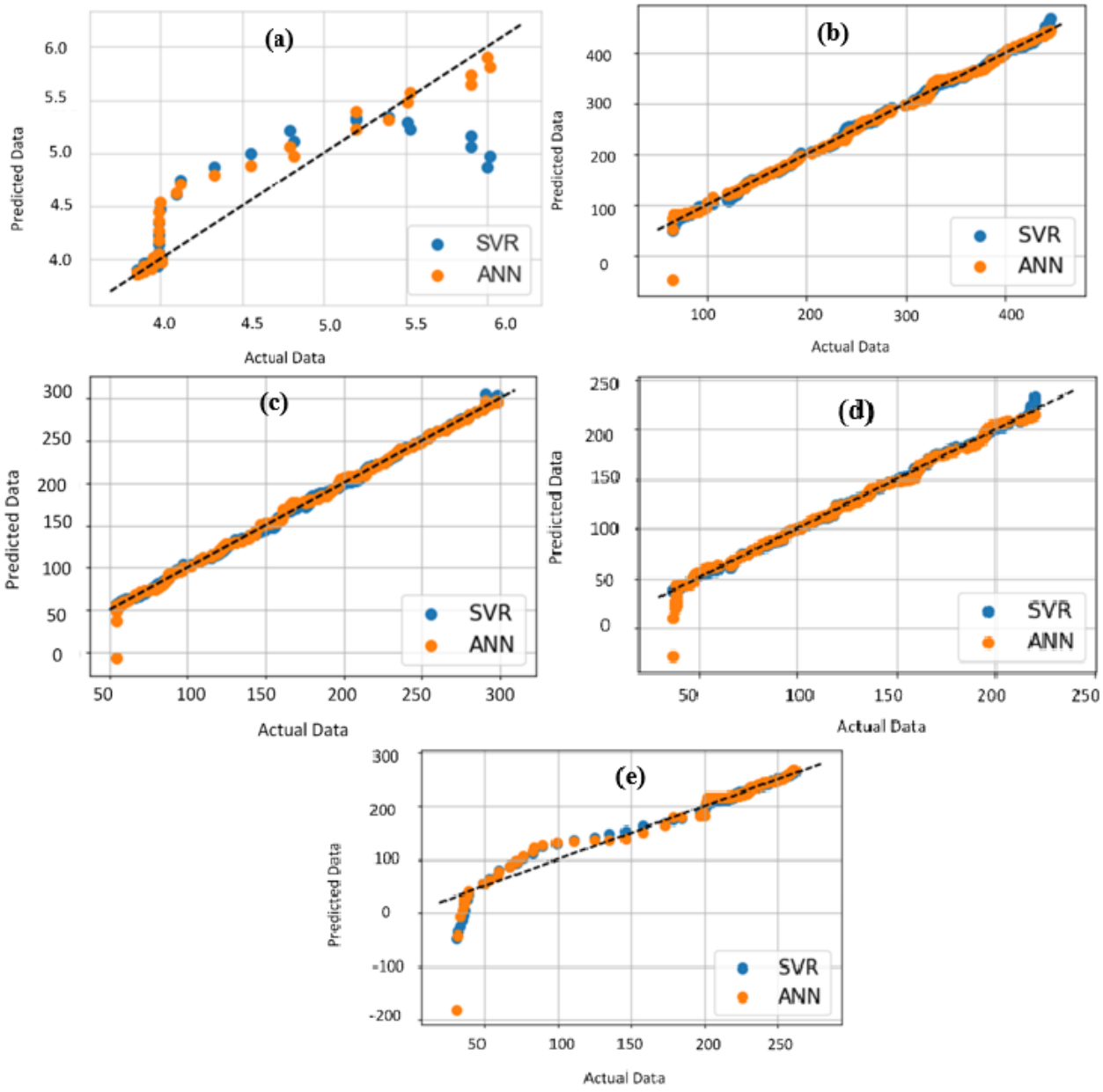

Figure 6. The predictive values by the SVR and ANN algorithms for (a) pH, (b) EC, (c) TDS, (d) salt, and (e) ORP factors.

4. Conclusion

In this work, the usability of ML method to predict the structural properties of drinking water treated by the plasma discharge was investigated. Before and after plasma treatment, the structural features of water such as pH, EC, TDS, salt, and ORP were experimentally measured according to operating conditions such as: treatment time and voltage applied on the needle electrode. The experimental setup and the measurements were expressed in section 2. In addition, the SVR algorithm of ML method and the determination procedure of hyperparameters used in this work was described in details. To confirm the accuracy and reliability of the SVR model, the MAE and *R*2 functions were calculated and the results were compared by those obtained by the ANN algorithm. It was found that MAE values in the prediction of the SVR model are lower than those of the ANN algorithm, and hence the prediction performance of the SVR algorithm is better than that of the ANN model. From Physical point of view, the change in liquid water characteristics is a result of the influence of reactive species and the physical conditions created at the air-water interface and into the water. Besides, the need for different experimental plasma treatments to find the best influencing on the structural properties of water were investigated. Changes in the structural characteristics of water depend on parameters such as the applied voltage and time of plasma exposure. It was seen that with the increase of applied voltage due to raise the electric field, the ionization process will be stronger and thus the EC, TDS, salt, and ORP is grown up while the values of pH are reduced. The parameter of time was also shown the same behavior, i.e. decreasing of pH and increasing of EC, TDS, salt, and ORP with the increase of the treatment time of plasma. By increasing the reactive species in the water

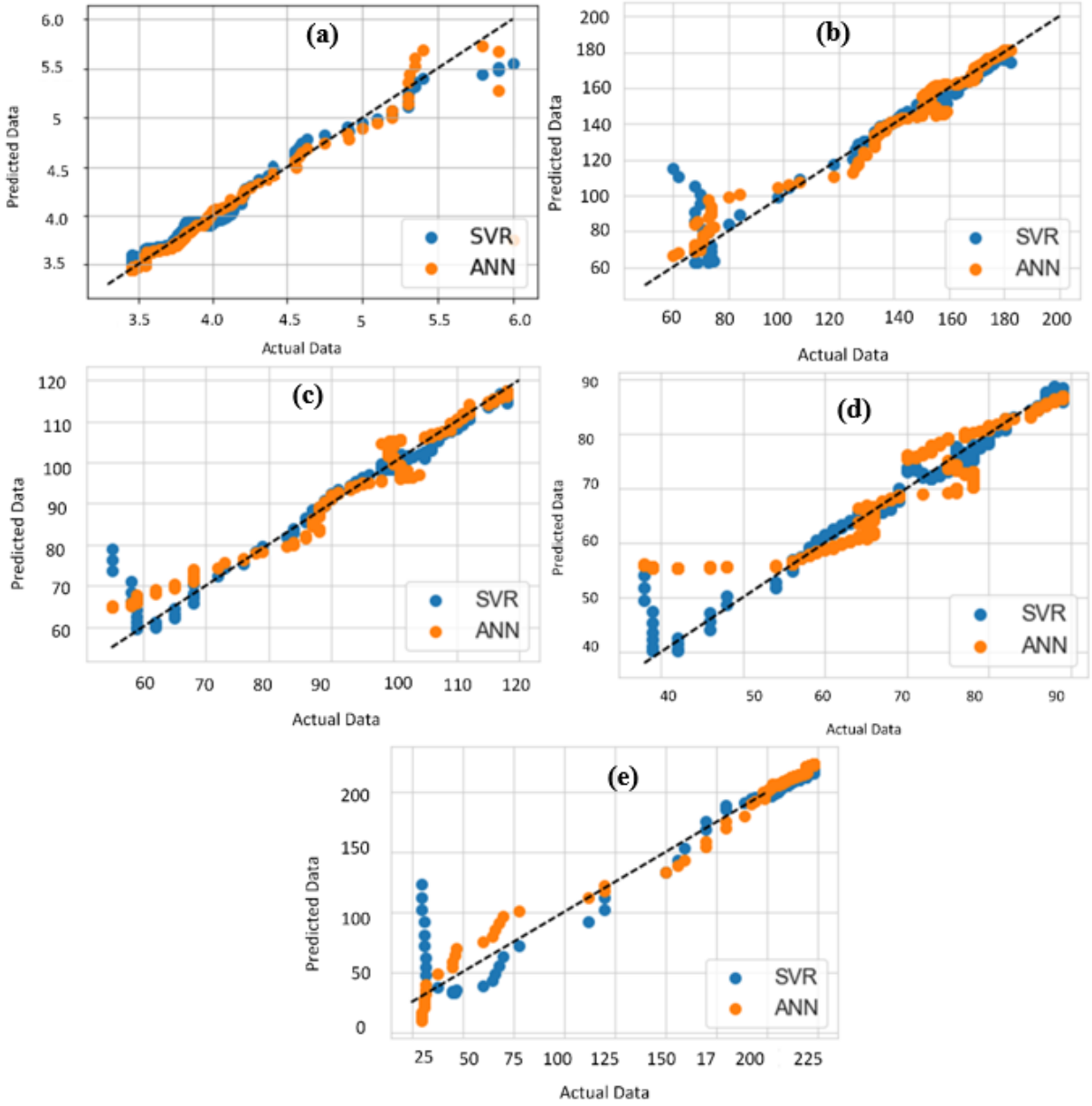

Figure 7. The predictive values by the SVR and ANN algorithms for (a) pH, (b) EC, (c) TDS, (d) salt, and (e) ORP factors.

after plasma treatment, the charge transfer mechanisms are facilitated and therefore the EC is raised. Moreover, the increase of the TDS and salt in the water is a result of growing the reactions up, originating from the increment of RONS in the medium. The decrease in pH values of the water is due to the increment of the concentration of H_3O^+, NO_2^-, and NO_3^- molecular species, as well as hydrogen ions, resulting in acidification of the water. At last, it is clear that the SVR algorithm is an accurate and reliable technique for predicting the structural characteristics of water exposed by plasma.

Authors Contributions

The author contribution is as follows: Saeed Karimian: Conceptualization, Experiment, Methodology, Writing-original draft; Shahrzad Falahat: Formal analysis, Software, Writing-original draft; Zahra Emam Bakhsh: Methodology, Discussion, Writing-original draft; Mohammad Javad Ghavami Rad: Experiment, Methodology, Writing-original draft; Ali Barkhordari: Investigation, Supervision, Project administration, Writing-review and editing.

Availability of Data and Materials

The datasets used and/or analyzed during the current study are available from the corresponding author upon reasonable request.

Conflict of Interests

The authors declare that they have no known competing financial interests or personal relationships that could have appeared to influence the work reported in this paper.

References

[1] M. C. García, M. Mora, D. Esquivel, J. E. Foster, A. Rodero, C. Jiménez-Sanchidrián, and F. J. Romero-Salguero. "Microwave atmospheric pressure plasma jets for wastewater treatment: degradation of methylene blue as a model dye. ". *Chemosphere*, **180**:239–246, 2017. DOI: https://doi.org/10.1016/j.chemosphere.2017.03.126.

[2] A. Barkhordari, S. Karimian, A. Rodero, D. A. Krawczyk, S. I. Mirzaei, and A. Falahat. "Carbon dioxide decomposition by a parallel-plate plasma reactor: experiments and 2-D modelling.". *Applied Sciences*, **11**:10047, 2021. DOI: https://doi.org/10.3390/app112110047.

[3] T. H. Martin, M. Williams, and M. Kristiansen. "JC Martin on pulsed power.". *Springer*, **3**, 2013.

[4] M. R. Webb and G. M. Hieftje. "Spectrochemical analysis by using discharge devices with solution electrodes. https://doi.org/". *Analytical Chemistry*, **81**: 862–7, 2009. DOI: https://doi.org/10.1021/ac801561t.

[5] A. Barkhordari, A. Ganjovi, I. Mirzaei, and A. Falahat. "Study of the physical discharge properties of a Ar/O_2 DC plasma jet. ". *Indian Journal of Physics*, **92**:1177–1186, 2018. DOI: https://doi.org/10.1007/s12648-018-1197-1.

[6] M. Smoluch, P. Mielczarek, and J. Silberring. "Plasma-based ambient ionization mass spectrometry in bioanalytical sciences. ". *Mass Spectrometry Reviews*, **35**:22–34, 2016. DOI: https://doi.org/10.1002/mas.21460.

[7] A. Barkhordari, S. Karimian, S. Shahsavari, D. Krawczyk, and A. Rodero. "Influence of the argon admixture on the reactive oxide species formation inside an atmospheric pressure oxygen plasma jet. ". *Scientific Reports*, **14**:3425, 2024. DOI: https://doi.org/10.1038/s41598-024-54111-y.

[8] J. Foster, B. S. Sommers, S. N. Gucker, I. M. Blankson, and G. Adamovsky. "Perspectives on the interaction of plasmas with liquid water for water purification.". *IEEE Transactions on Plasma Science*, **40**:1311–1323, 2012. DOI: https://doi.org/10.1109/TPS.2011.2180028.

[9] D. Mariotti, J. Patel, V. Švrček, and P. Maguire. "Plasma–liquid interactions at atmospheric pressure for nanomaterials synthesis and surface engineering. ". *Plasma Processes and Polymers*, **9**:1074–1085, 2012. DOI: https://doi.org/10.1002/ppap.201200007.

[10] T. Ishijima, K. Nosaka, Y. Tanaka, Y. Uesugi, Y. Goto, and H. Horibe. "A high-speed photoresist removal process using multibubble microwave plasma under a mixture of multiphase plasma environment. ". *Applied Physics Letters*, **103**, 2013. DOI: https://doi.org/10.1063/1.4823530.

[11] A. Barkhordari, S. I. Mirzaei, A. Falahat, and A. Rodero. "Numerical and experimental study of an Ar/CO_2 plasma in a point-to-plane reactor at atmospheric pressure. ". *Spectrochimica Acta Part B: Atomic Spectroscopy*, **177**:106048, 2021. DOI: https://doi.org/10.1016/j.sab.2020.106048.

[12] J. F. Friedrich, R. Mix, R. D. Schulze, A. Meyer-Plath, R. Joshi, and S. Wettmarshausen. "New plasma techniques for polymer surface modification with monotype functional groups. ". *Plasma Processes and Polymers*, **5**:407–423, 2008. DOI: https://doi.org/10.1002/ppap.200700145.

[13] P. J. Bruggeman and B. R. Locke. "Assessment of potential applications of plasma with liquid water. ". *Low Temperature Plasma Technology: Methods and Applications.*, :367–399, 2013.

[14] G. Fridman, G. Friedman, A. Gutsol, A. B. Shekhter, V. N. Vasilets, and A. Fridman. "Applied plasma medicine. ". *Plasma Processes and Polymers*, **5**:503–533, 2008. DOI: https://doi.org/10.1002/ppap.200700154.

[15] E. H. Houssein, Z. Abohashima, M. Elhoseny, and W. M. Mohamed. "Machine learning in the quantum realm: The state-of-the-art, challenges, and future vision. ". *Expert Systems with Applications*, **194**:116512, 2022. DOI: https://doi.org/10.1016/j.eswa.2022.116512.

[16] V. Vapnik. "The nature of statistical learning theory.". *Springer*, , 2013.

[17] C. W. Hsu, C. C. Chang, and C. J. Lin. "A practical guide to support vector classification.". , 2003.

[18] E. Ahmadloo and S. Azizi. "Prediction of thermal conductivity of various nanofluids using artificial neural network. ". *International Communications in Heat and Mass Transfer*, **74**:69–75, 2016. DOI: https://doi.org/10.1016/j.icheatmasstransfer.2016.03.008.

[19] M. Awad and R. Khanna. "Efficient learning machines: theories, concepts, and applications for engineers and system designers. ". *Springer*, :268, 2015.

[20] M. Rupp, A. Tkatchenko, K. R. Müller, and O. A. Von Lilienfeld. "Fast and accurate modeling of molecular atomization energies with machine learning. ". *Physical Review Letters*, **108**:058301, 2012. DOI: https://doi.org/10.1103/PhysRevLett.108.058301.

[21] R. Zhang and W. Wang. "Facilitating the applications of support vector machine by using a new kernel.". *Expert Systems With Applications*, **38**:14225–14230, 2011. DOI: https://doi.org/10.1016/j.eswa.2011.04.235.

[22] P. Bruggeman and D. C. Schram. "On OH production in water containing atmospheric pressure plasmas.". *Plasma Sources Science and Technology*, **19**, 2010. DOI: https://doi.org/10.1088/0963-0252/19/4/045025.

[23] A. Barkhordari, S. I. Mirzaei, A. Falahat, D. A. Krawczyk, and A. Rodero. "Experimental study of a rotating electrode plasma reactor for hydrogen production from liquid petroleum gas conversion.". *Applied Sciences*, **12**:4045, 2022. DOI: https://doi.org/10.3390/app12084045.

[24] V. A. Titov, V. V. Rybkin, S. A. Smirnov, A. N. Kulentsan, and H. S. Choi. ". Experimental and theoretical studies on the characteristics of atmospheric pressure glow discharge with liquid cathode. ". *Plasma Chemistry and Plasma Processing*, **26**:543–555, 2006. DOI: https://doi.org/10.1007/s11090-006-9014-6.

[25] A. Barkhordari, A. Ganjovi, I. Mirzaei, A. Falahat, and M. N. Rostami Ravari. "A pulsed plasma jet with the various Ar/N_2 mixtures.". *Journal of Theoretical and Applied Physics*, **11**:301–312, 2017. DOI: https://doi.org/10.1007/s40094-017-0271-y.

[26] S. A. Norberg, W. Tian, E. Johnsen, and M. J. Kushner. "Atmospheric pressure plasma jets interacting with liquid covered tissue: touching and not-touching the liquid.". *Journal of Physics D: Applied Physics*, **47**:475203, 2014. DOI: https://doi.org/10.1088/0022-3727/47/47/475203.

[27] W. Tian and M. J. Kushner. "Atmospheric pressure dielectric barrier discharges interacting with liquid covered tissue. ". *Journal of Physics D: Applied Physics*, **47**:165201, 2014. DOI: https://doi.org/10.1088/0022-3727/47/16/165201.

[28] D. Minakata, K. Li, P. Westerhoff, and J. Crittenden. "Development of a group contribution method to predict aqueous phase hydroxyl radical (HO•) reaction rate constants.". *Environmental Science & Technology*, **43**:6220–6227, 2009. DOI: https://doi.org/10.1021/es900956c.

[29] T. Cserfalvi and P. Mezei. "Operating mechanism of the electrolyte cathode atmospheric glow discharge. ". *Fresenius' Journal of Analytical Chemistry*, **355**:813–819, 1996. DOI: https://doi.org/10.1007/s0021663550813.

[30] A. F. Gaisin and E. E. E. Son. "Vapor-air discharges between electrolytic cathode and metal anode at atmospheric pressure. ". *High Temperature*, **43**:1–7, 2005. DOI: https://doi.org/10.1007/PL00021849.

[31] P. Wardman. "Fluorescent and luminescent probes for measurement of oxidative and nitrosative species in cells and tissues: progress, pitfalls, and prospects. ". *Free Radical Biology & Medicine*, **43**:995–1022, 2007. DOI: https://doi.org/10.1016/j.freeradbiomed.2007.06.026.

[32] M. Anbar and H. Taube. ". Interaction of nitrous acid with hydrogen peroxide and with water. ". *Journal of the American Chemical Society*, **76**:6243–6247, 1954. DOI: https://doi.org/10.1021/ja01653a007.

[33] K. Oehmigen, J. Winter, M. Hähnel, C. Wilke, R. Brandenburg, K. D. Weltmann, and T. von Woedtke. "Estimation of possible mechanisms of Escherichia coli inactivation by plasma treated sodium chloride solution. ". *Plasma Processes and Polymers*, **8**:904–913, 2011. DOI: https://doi.org/10.1002/ppap.201000099.

[34] S. Goldstein, J. Lind, and G. Merényi. "Chemistry of peroxynitrites as compared to peroxynitrates. ". *Chemical Reviews*, **105**:2457–2470, 2005. DOI: https://doi.org/10.1021/cr0307087.

[35] M. M. Turner. ". Uncertainty and sensitivity analysis in complex plasma chemistry models. ". *Plasma Sources Science and Technology*, **25**:015003, 2015. DOI: https://doi.org/10.1088/0963-0252/25/1/015003.